

Punching shear tests of normal- and high-strength concrete flat plates

Sevket Ozden, Ugur Ersoy, and Turan Ozturan

Abstract: Experimental research was conducted to investigate the punching shear performance of flat plates. A large number of slab specimens of normal- and high-strength concrete were tested under concentric and eccentric loads. The effects of flexural reinforcement and the use of steel fiber reinforcement were investigated. Experimental expressions were developed for the computation of residual slab strength. Experimentally observed punching shear capacities were compared with those from the provisions of Canadian Standards Association (CSA) standard CSA-A23.3-04. The results indicate that concrete strength plays an important role in punching capacity and slab rigidity. Slabs with a higher percentage of flexural reinforcement show an increase in punching capacity. The use of steel fibers results in improved strength and stiffness while also enhancing the postpeak deformability and residual strength. The empirical expressions developed provide reasonably good predictions of residual slab capacities. CSA-A23.3-04 expressions result in conservative punching shear capacity predictions for concentrically loaded slabs and provide good agreement with the experimentally observed punching shear capacities for eccentrically loaded slabs.

Key words: reinforced concrete, flat plate, punching shear, strength, high-strength concrete, eccentric loading, slab reinforcement ratio, steel fiber reinforced concrete.

Résumé : Une recherche expérimentale a étudié le rendement des dalles pleines sous une cisaille-poinçonneuse. Un grand nombre d'échantillons de dalles en béton armé de résistance normale et à haute résistance ont été testés sous des charges concentriques et excentrées. Les effets du renforcement en flexion et l'utilisation du renforcement par fibres d'acier ont été examinés. Les expressions expérimentales ont été mises sur pied pour calculer la résistance résiduelle des dalles. Les capacités de résistance sous une cisaille-poinçonneuse observées lors de l'expérience ont été comparées aux dispositions de la norme CSA A23.3-04. Les résultats montrent que la résistance du béton joue un rôle important dans la résistance au poinçonnement et dans la rigidité de la dalle. Les dalles comportant un plus haut pourcentage de renforcement en flexion montrent une capacité accrue de résistance au poinçonnement. L'utilisation des fibres d'acier accroît la résistance et la rigidité tout en augmentant la déformabilité post pic et la résistance résiduelle. Les expressions empiriques développées fournissent des prévisions raisonnablement précises des capacités résiduelles des dalles. Les équations dans la norme CSA A23.3-04 engendrent des prévisions conservatrices de la capacité de résistance au poinçonnement pour les dalles sous charges concentriques tout en fournissant une bonne corrélation pour les dalles sous charges excentrées.

Mots clés : béton armé, dalle pleine, cisaille-poinçonneuse, résistance, béton à haute résistance, charge excentrée, pourcentage d'armature des dalles, béton armé de fibres d'acier.

[Traduit par la Rédaction]

Introduction

A major aspect of the design of reinforced concrete flat-plate floor systems involves safety against punching shear. Punching shear stresses may reach critical levels in flat plate

to column connections under gravity loads (Zaghlool and de Paiva 1973) that may be imposed in combination with unbalanced moments caused by patterned gravity loads and (or) lateral loads due to earthquakes.

Extensive experimental and analytical studies have been carried out over the years to investigate different aspects of punching shear failures in flat plates, where the potential failure modes range from pure punching to pure bending to a combination of the two. The published experimental research on this topic can be divided into two main categories: (i) isolated slab-column tests (e.g., Moe 1961; Hanson and Hanson 1968; Ozselcuk 1980; Halgren and Kinnunen 1993; Ozden 1998), and (ii) tests on slab systems (Hatcher et al. 1961; Tankut and Yu 1969; Pecknold 1975). The majority of experimental investigations were carried out on isolated specimens. The determination of punching load capacity was of prime importance in both categories of research. The previous research indicates that isolated punching tests represent the punching behavior of interior slab-column connections in

Received 23 January 2006. Revision accepted 12 June 2006.
Published on the NRC Research Press Web site at <http://cjce.nrc.ca> on 24 January 2007.

S. Ozden.¹ Department of Civil Engineering, Kocaeli University, Veziroğlu Kampüsü, Kocaeli, Turkey.

U. Ersoy. Department of Civil Engineering, Middle East Technical University, Ankara, Turkey.

T. Ozturan. Department of Civil Engineering, Bogazici University, Istanbul, Turkey.

Written discussion of this article is welcomed and will be received by the Editor until 31 March 2007.

¹Corresponding author (e-mail: sevketozden@yahoo.com).

continuous flat-plate systems reasonably well (Gardner and Shao 1996).

The use of high-strength concrete (HSC) has increased significantly in recent years. Despite the widespread use of HSC in building construction, limited information has become available on the structural performance of this new material. Several researchers have pointed out that the adequacy of the available building code design equations for HSC must be questioned to ensure safety and serviceability of buildings (Marzouk and Hussein 1991; Ramdane 1996). The concern for punching shear is not only the relative level of strength, but also the change in behavior of concrete with increasing compressive strengths. Test results show that complicated design equations, such as that proposed by Moe (as cited in CED–fib Task Group 2001) and classified as a flexural capacity approach, overestimate the punching shear capacity of HSC flat plates (Marzouk and Hussein 1991). The published research reveals that using the cubic root of concrete compressive strength generally yields better results in predicting plate capacity (Gardner 1990; Gomes and Andrade 1996; Ramdane 1996). Test results further reveal that an increase in concrete compressive strength affects the punching behavior significantly. In the post-failure region, the aggregate interlock effect is reduced in HSC slabs as compared to normal-strength concrete (NSC) slabs (Halgren and Kinnunen 1996). Increasing concrete strength leads to an increase in punching shear resistance of a flat plate but may not necessarily indicate a change in failure surface location and geometry (Gomes and Andrade 1996). It has also been reported that the appearance of flexural cracks is delayed when HSC is used (Ramdane 1996), and the stiffness of flat plates increases with an increase in concrete strength, but at a much lower rate than the changing rate of $(f'_c)^{1/2}$ (Marzouk and Hussein 1991), where f'_c is the compressive strength of a standard 150 mm × 300 mm concrete cylinder.

Slab–column connections in flat-plate structures carry a combination of shear and unbalanced moments, which are unavoidable at the edge and corner columns and may occur at interior columns as a result of unequal spans, patterned loading, and lateral loading. Unbalanced moments are transferred from the column to the slab by flexural and torsional resistance of vertical slab–column interfaces. As gravity loads increase, the remaining shear capacity is reduced to resist unbalanced moments (Pan and Moehle 1992). The proportion of moment transferred through shear in building codes is either formulated as being proportional to the column aspect ratio or taken as a constant fraction. It has been shown that in transferring the moment the participation of torsional, flexural, and shear stresses depends on the shape and size of the column (Mast 1970). Moreover, experiments show that the proportion of moment transferred through shear decreases with an increase in the steel ratio in the column strip (Lou and Durrani 1995).

In addition to the previously mentioned variables, there is experimental and analytical evidence that punching shear strength is also affected by the dimensional ratios between the column and the plate. The ability of a slab to resist unit shear stress diminishes as the size of the loaded area increases relative to slab thickness (Moe 1961; Rao and Goli 1985; Paramasivam and Tan 1993). The ratio of critical punching perimeter to the effective slab depth is also

claimed to have an effect on the punching shear strength. For typical small values of this ratio, the most stressed region of the plate-to-column connection is well confined by in-plane stresses. For larger ratios, the confinement of the punching zone is likely to be reduced, resulting in a decrease in shear strength (Moehle et al. 1988). The code design equations and some plate models are reported to be valid for column cross-sectional dimension to slab depth ratios of less than three (Vanderbilt 1972). The column shape and aspect ratio also have an influence on the punching strength. It is reported that the strength of slabs with circular columns is greater than that of slabs with square columns having identical dimensional and reinforcement ratios (Shilling and Vanderbilt 1970; Vanderbilt 1972). As the aspect ratio of a column increases, the abruptness of failure increases, and the size of the failure cone decreases (Hawkins and Mitchell 1979). Experiments show that punching shear strength for loading through rectangular areas with aspect ratios greater than two is less than that for loading through square areas. Slab overall dimensions may also have an influence on the punching shear strength. It is observed that shear strength increases significantly as the shear span to shear depth ratio decreases below three (Lovrovich and McLean 1990). On the other hand, increasing this ratio seems to have little effect, if any, on strength (Paramasivam and Tan 1993). Furthermore, experimental investigations on large-scale isolated specimens indicate that the size effect in tests becomes significant when the scale of the model is less than one-quarter that of the prototype (Neth et al. 1981).

Another parameter that may affect the performance of slabs is the use of steel fiber reinforcement (SFR). Structural elements subjected to tensile stresses, including regions under moment- or shear-induced tensile stresses, may experience altered stress flow with the addition of SFR. Prior to cracking, the tensile stresses are shared by the fiber and the matrix. As cracking starts, the stress is progressively transferred to the fibers as they bridge the cracks and prevent them from widening. Therefore, SFR may be used to improve the punching shear capacities of flat-plate structures (Ghalib 1980; Swamy and Ali 1982; Alexander and Simmonds 1992; Theodorakopoulos and Swamy 1993). Experimental observations indicate that flat plates with SFR develop reduced deformations and enhanced punching shear capacities while experiencing a substantial reduction in tensile strains of the main slab reinforcement (Swamy and Ali 1982).

Experimental program

Extensive testing of half-scale reinforced concrete flat plates was conducted to investigate the significance of design parameters on the punching shear behavior of slabs. The experimental program consisted of a total of 26 reinforced concrete flat plates tested under monotonically increasing punching loads. The slab plates had a 1500 mm diameter circular geometry and 120 mm thickness with a concentric 200 mm square central column stub, extending above and below the slab (Ozden 1998). The specimens were supported along their perimeter by uniformly spaced tie rods, placed 600 mm away from the center of the column stub. The average effective slab depth was $d = 100$ mm, measured to the centroid of tension steel. The compression

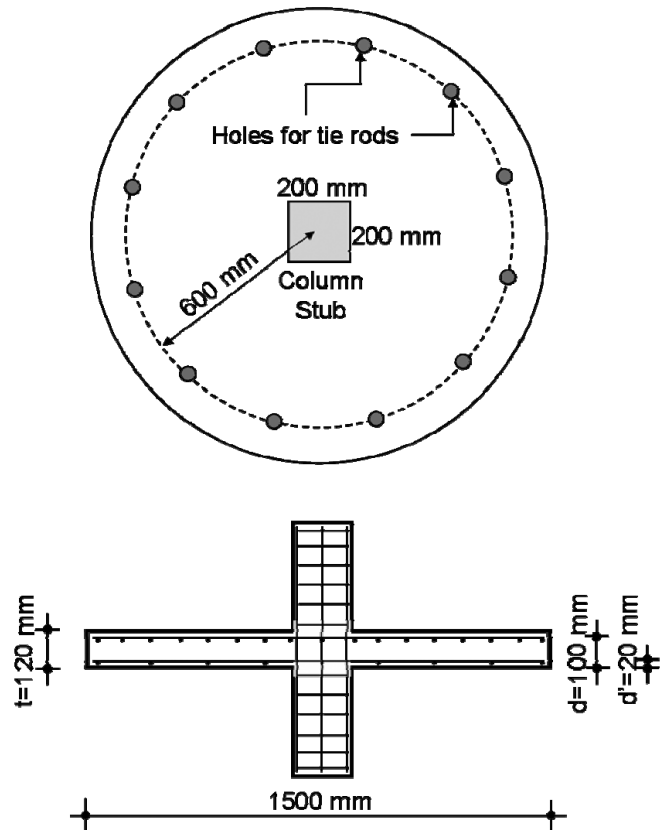
reinforcement was placed at a distance $d' = 20$ mm from the extreme compression fiber, measured to the centroid of reinforcement. The geometric details of the test specimens are shown in Fig. 1.

Two different target concrete strengths were used, representing NSC and HSC with strengths of 20 and 80 MPa, respectively, although there were some variations in strength among different batches, as indicated in Table 1. Each specimen was reinforced with two orthogonal layers of reinforcement. The NSC specimens had 10 mm diameter deformed bars, top and bottom, whereas the HSC specimens had 14 mm diameter deformed bars, with yield strengths of 507 and 471 MPa, respectively. The spacing of the top layer (tension reinforcement) was twice that of the bottom layer (compression reinforcement). Figure 2 provides the details of slab reinforcement, also indicating that two reinforcement ratios were used for each group of NSC and HSC specimens. The specimens were labeled to reflect the test parameters. The first letter in the label indicates the concrete strength (N for NSC and H for HSC). The second entry in the label (R1 or R2) indicates the ratio of flexural strength to punching strength (P_{flex}/P_{ACI}), where the flexural strength (P_{flex}) was calculated using yield line analysis, and the nominal punching shear strength (P_{ACI}) was calculated using the ACI-318-02 provisions (ACI Committee 318 2002). R1 indicates a P_{flex}/P_{ACI} ratio of 1.1, and R2 a ratio of 1.6. These different ratios were achieved by using two different reinforcement ratios. The third entry in the specimen label represents the eccentricity of the load. The designation of E0 indicates zero eccentricity (concentric loading), E1 indicates an eccentricity of 100 mm (equal to half the column dimension), and E2 indicates an eccentricity of 200 mm (equal to the column dimension). The last entry in the label indicates the presence of SRF. F0 is used for specimens without SFR and F1 for specimens with 75 kg of hooked-end SFR per cubic metre of concrete (approximately 1% fiber by volume, or $V_{TF} = 1\%$). The yield strength of SFR was specified by the producer to be greater than 1100 MPa. Table 1 provides a summary of the specimens tested, the test parameters considered, and the properties of the specimens.

Test setup and instrumentation

Figure 3 illustrates the experimental setup used for testing the slabs. The specimens were supported along their perimeter by 12 evenly spaced tie rods, connecting the slabs to a reinforced concrete reaction block. The circular reaction block had a diameter of 1200 mm and thickness of 360 mm. Tie rods with bolted ends were secured to specimens through the holes along the perimeter and were connected to the reaction block. Monotonically increasing load was applied by a hydraulic ram with a capacity of 1000 kN through a semi-spherical seat mounted directly on the bottom of the column. The rate of oil flow to the hydraulic ram was kept at a minimum to trace the post-failure behavior of the plates, as the tests were conducted in the load-control mode. The eccentricity of the load was kept at most at 200 mm to ensure continuous tension in all tie rods. A steel loading arm was used for eccentric loading. A load cell, placed between the hydraulic ram and the roller support, was used to measure the applied load. The roller support for eccentrically loaded specimens allowed rotation along one axis. The eccentricity

Fig. 1. Dimensions of the test specimens.



was measured from the center of the column to the center of the roller support. Displacements were measured at seven different locations along the diameter of plates by means of linearly variable displacement transducers (LVDTs). This is illustrated in Fig. 3. Loads and displacements were recorded at every second of loading by means of an electronic data acquisition system, as the applied load versus slab center deflection was monitored on a computer monitor during testing. The progression of cracks was marked at certain intervals. A sudden drop in load was recorded when the slab punched through, with the exception of NSC specimens with SFR. Although the failure point was defined as a significant drop in load resistance, testing continued until another equilibrium point was attained at a lower level of load. This was called the residual strength and designated as P_{re} . The load capacity of specimens started increasing once again at very large slab deformations because of the membrane action and the strain hardening of the slab reinforcement. Testing terminated at approximately this stage of loading.

Test results

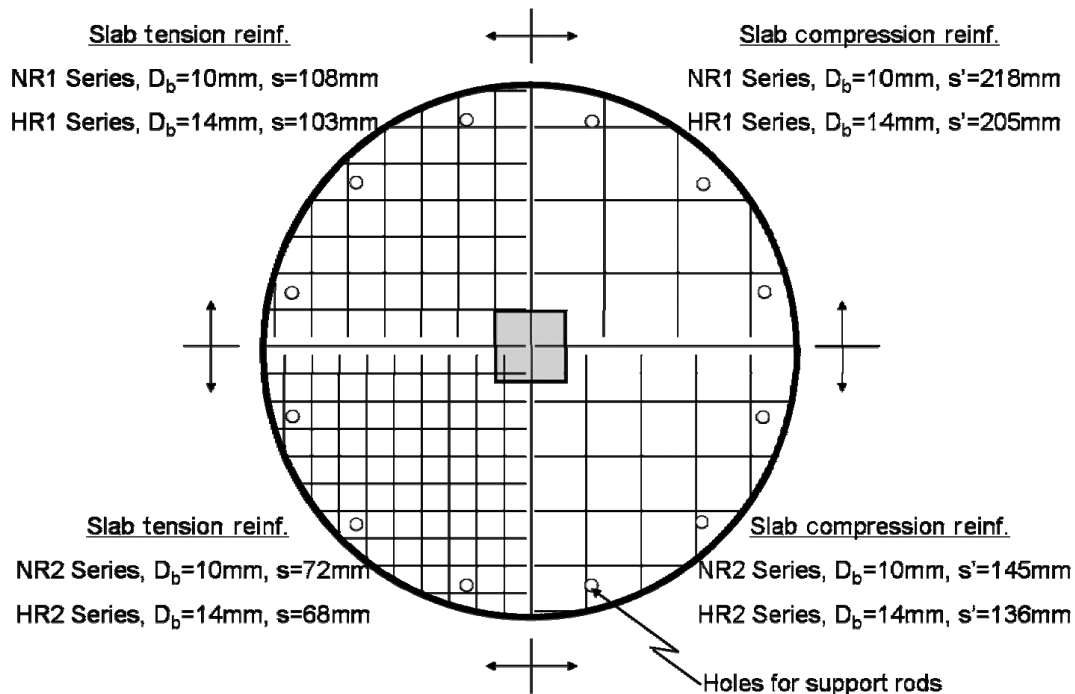
Behavior of test specimens

The behavior of specimens is discussed with reference to observed crack patterns. Four different types of cracks were observed on the tension face of slabs and are denoted F, P, Q, and R cracks, as illustrated in Fig. 4. When the tensile strength of concrete in flexure was reached, cracks parallel to the column face on the tension side were observed near the vicinity of the column stub. These were designated as F

Table 1. Properties of test specimens and test results.

Specimen	f'_c (MPa)	f_{sp} (MPa)	ρ (%)	V_{IF} (%)	e (mm)	P_{cr} (kN)	δ_{cr} (mm)	P_p (kN)	δ_p (mm)	P_{re} (kN)
NR1E0F0	21.6	2.33	0.73	0.0	0	49	0.25	188	6.35	63
NR1E1F0	19.3	2.38	0.73	0.0	100	42	0.30	159	5.50	65
NR1E2F0	18.5	2.21	0.73	0.0	200	36	0.27	118	4.90	49
NR2E0F0	20.0	2.34	1.09	0.0	0	71	0.60	202	5.50	78
NR2E1F0	20.9	2.41	1.09	0.0	100	52	0.39	178	4.70	79
NR2E2F0	20.1	2.27	1.09	0.0	200	44	0.34	130	3.47	66
HR1E0F0	74.0	4.58	1.50	0.0	0	107	0.47	331	5.75	136
HR1E0F0r	75.0	4.93	1.50	0.0	0	136	0.64	371	5.43	159
HR1E1F0	75.0	4.93	1.50	0.0	100	127	0.47	357	5.18	146
HR1E2F0	75.0	4.93	1.50	0.0	200	105	0.46	262	4.49	118
HR2E0F0	63.7	4.12	2.25	0.0	0	120	0.25	405	3.82	175
HR2E0F0r	74.7	4.81	2.25	0.0	0	126	0.58	489	6.42	177
HR2E1F0	74.7	4.81	2.25	0.0	100	120	0.42	396	4.48	162
HR2E2F0	74.7	4.81	2.25	0.0	200	88	0.31	327	3.86	164
NR1E0F1	19.6	2.44	0.73	1.0	0	59	0.32	266	7.54	155
NR1E1F1	19.6	2.44	0.73	1.0	100	55	0.29	211	7.66	125
NR1E2F1	19.6	2.44	0.73	1.0	200	54	0.16	188	5.82	96
NR2E0F1	19.3	2.49	1.09	1.0	0	87	0.53	245	5.69	172
NR2E1F1	19.3	2.49	1.09	1.0	100	79	0.46	192	3.93	150
NR2E2F1	19.3	2.49	1.09	1.0	200	57	0.45	142	4.91	105
HR1E0F1	81.3	6.84	1.50	1.0	0	132	0.45	576	10.80	275
HR1E1F1	81.3	6.84	1.50	1.0	100	126	0.35	405	7.47	—
HR1E2F1	81.3	6.84	1.50	1.0	200	126	0.48	369	8.72	210
HR2E0F1	79.3	7.03	2.25	1.0	0	185	0.61	691	7.78	295
HR2E1F1	79.3	7.03	2.25	1.0	100	160	0.59	528	7.60	265
HR2E2F1	79.3	7.03	2.25	1.0	200	150	0.72	411	5.76	—

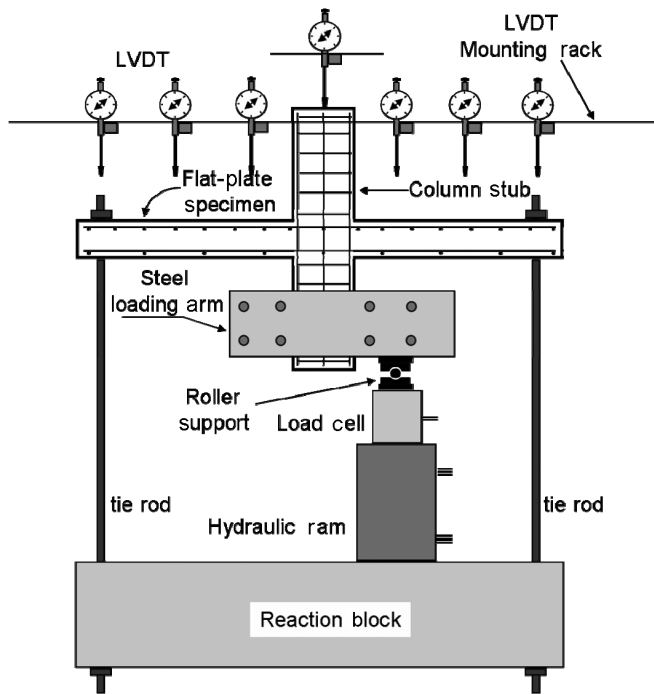
Note: Slab and column dimensions were identical in all test specimens (see Fig. 1). Parameters as defined in the List of symbols.

Fig. 2. Slab reinforcement (reinf.) details.

cracks. The load at which these cracks were observed was labelled as P_{cr} , and the corresponding displacement as δ_{cr} . Although the F cracks formed parallel to each column face in concentrically loaded specimens, they were observed only

along the tension face of the column in eccentrically loaded specimens. In either case, the F cracks were observed at a distance of approximately 5–10 mm from the column face. The formation of radial cracks was observed after the forma-

Fig. 3. Loading system and instrumentation.

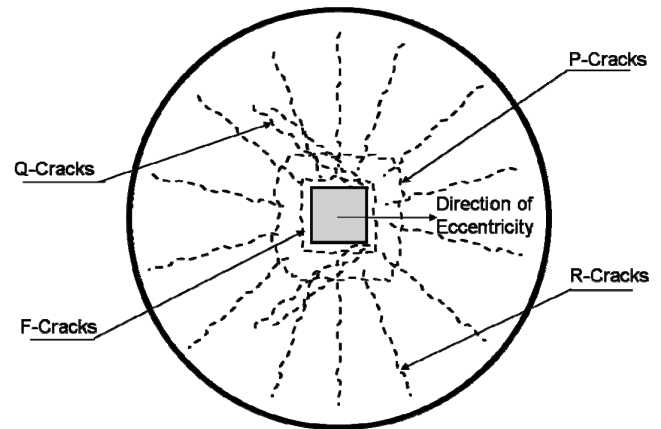


tion of F cracks, initiated at column corners. These cracks are referred to as R cracks. The R cracks propagated towards the slab boundary under increasing loads as new radial cracks initiated from the column edges.

At later stages of loading, new cracks formed parallel to column faces. These cracks are referred to as P cracks. They were located consistently at a distance of approximately 100 mm (equal to effective slab depth) from the column face in all specimens. These cracks formed parallel to each column face in concentrically loaded columns, whereas they formed only in the direction of eccentricity under eccentric loading. Punching shear failure under concentric loading took place as a result of the opening of P cracks around columns, whereas in eccentrically loaded specimens it occurred along P and Q cracks, where Q cracks initiated at column side faces and propagated towards the opposite direction of the eccentricity, forming an angle with the column side faces. The failure load was defined as P_p . Q cracks were observed only in eccentrically loaded specimens and appeared after the formation of initial F cracks. Inclined Q cracks propagated towards the slab boundaries under increasing loads. The Q cracks in eccentrically loaded specimens eventually joined the P cracks, triggering a punching failure.

Crack patterns of specimens without SFR are shown in Fig. 5 at the end of testing. The patterns for specimens with SFR are illustrated in Fig. 6. It is observed that the crack density in NSC and HSC specimens is closely related to the spacing of slab flexural reinforcement. Closer bar spacing resulted in smaller crack spacing, as expected, regardless of the presence of SFR. The presence of SFR controlled cracking outside the failure region, however, resulting in a larger undamaged zone that provided more effective confining stresses on the failure surface, affecting the ultimate failure load. Some of the R cracks traveled close to the plate boundaries in the absence of SFR, in contrast to specimens with

Fig. 4. Typical crack patterns on slab tension side.



SFR, in which the R cracks were confined in an encircled zone, as illustrated in Figs. 5 and 6. Specimens with SFR had more cracks with a smaller width as compared with companion specimens without SFR.

Strength and deformation of test specimens

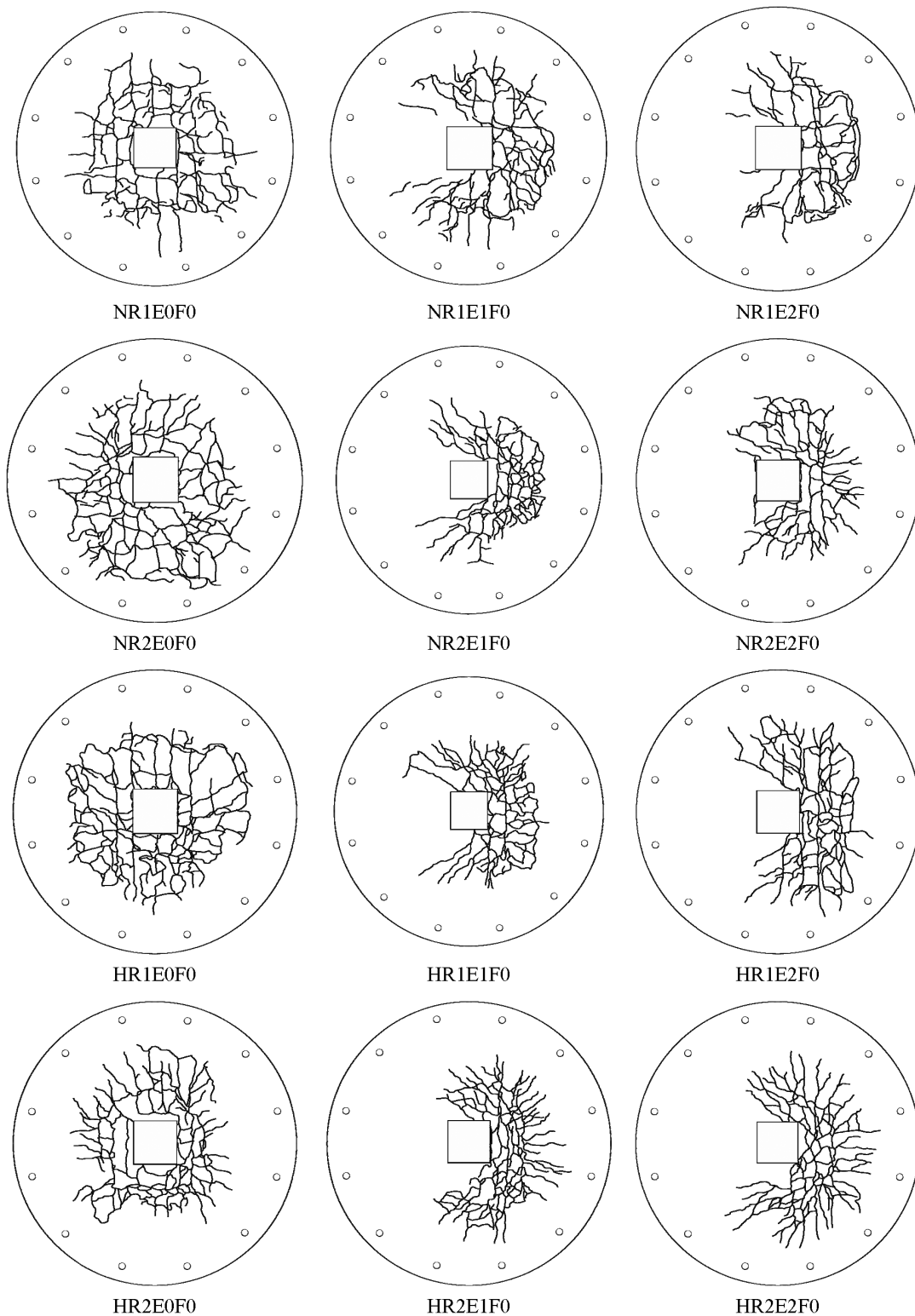
Experimentally recorded loads at first cracking (P_{cr}), punching failure (P_p), and residual strength (P_{re}) are summarized in Table 1 for each specimen, with the corresponding deflections at plate center. Load–displacement curves of the test specimens are shown in Fig. 7. The displacements shown in Fig. 7 are those measured at the plate center relative to the supports.

The center deflections indicated that an increase in the eccentricity of the load resulted in a smaller deflection at failure, regardless of concrete strength, reinforcement ratio, and SFR content. This was attributed to the lower failure loads observed in eccentrically loaded specimens as compared with those tested under concentric loading. When post-cracking slopes of load–deflection curves are compared, it is observed that the deflection under a given load increased with a decrease in eccentricity. Test results further indicate that deflections decreased with an increase in concrete strength, regardless of other variables. For the same load level and P_{flex}/P_{ACI} ratio, the deflections of NSC specimens were approximately twice those of HSC specimens. The addition of SFR to slab concrete reduced deflection at the same level of load.

Post-failure behavior and residual load capacity

A drop in load was observed in all specimens beyond the peak failure load, P_p . This drop in load was stabilized at a certain level (P_{re}), beyond which the specimens continued carrying approximately the same level of load under increasing deflections. The post-failure behavior was highly influenced by fiber content, concrete compressive strength, slab reinforcement ratio, and eccentricity of the load. In NSC specimens without SFR, the drop in load after failure was relatively gradual, regardless of slab reinforcement ratio. For eccentricities less than 200 mm, these specimens experienced a more gradual drop in load. HSC specimens showed a more brittle post-failure behavior. This was true whether the load was concentric or eccentric. Under eccentric loading, how-

Fig. 5. Crack pattern of specimens without SFR after testing.

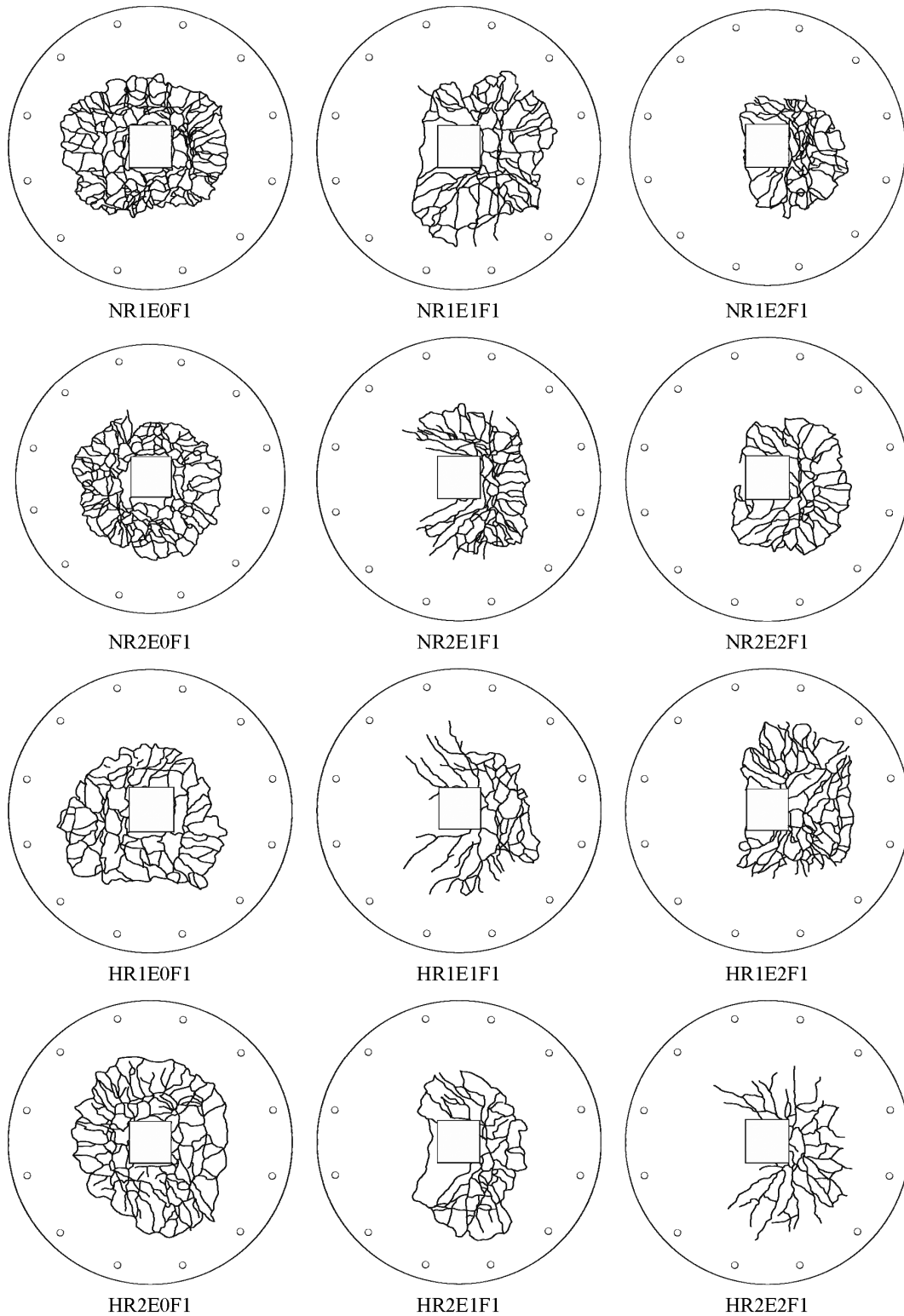


ever, HSC specimens experienced faster degradation when the slab reinforcement ratio was increased.

The post-failure region of the load–deflection curves was also influenced by the presence of fiber reinforcement. NSC specimens showed more gradual strength decay when SFR was used, regardless of slab reinforcement ratio and eccen-

tricity. Furthermore, the slab reinforcement crossing punching perimeter appeared to have a positive effect on post-failure resistance due to dowel action. The reinforcement crossing punching perimeter was proportional to the ratio of slab tension reinforcement, ρ , in all specimens, and bar spacing varied with changes in ρ , since the same size bars were

Fig. 6. Crack pattern of specimens with SFR after testing.

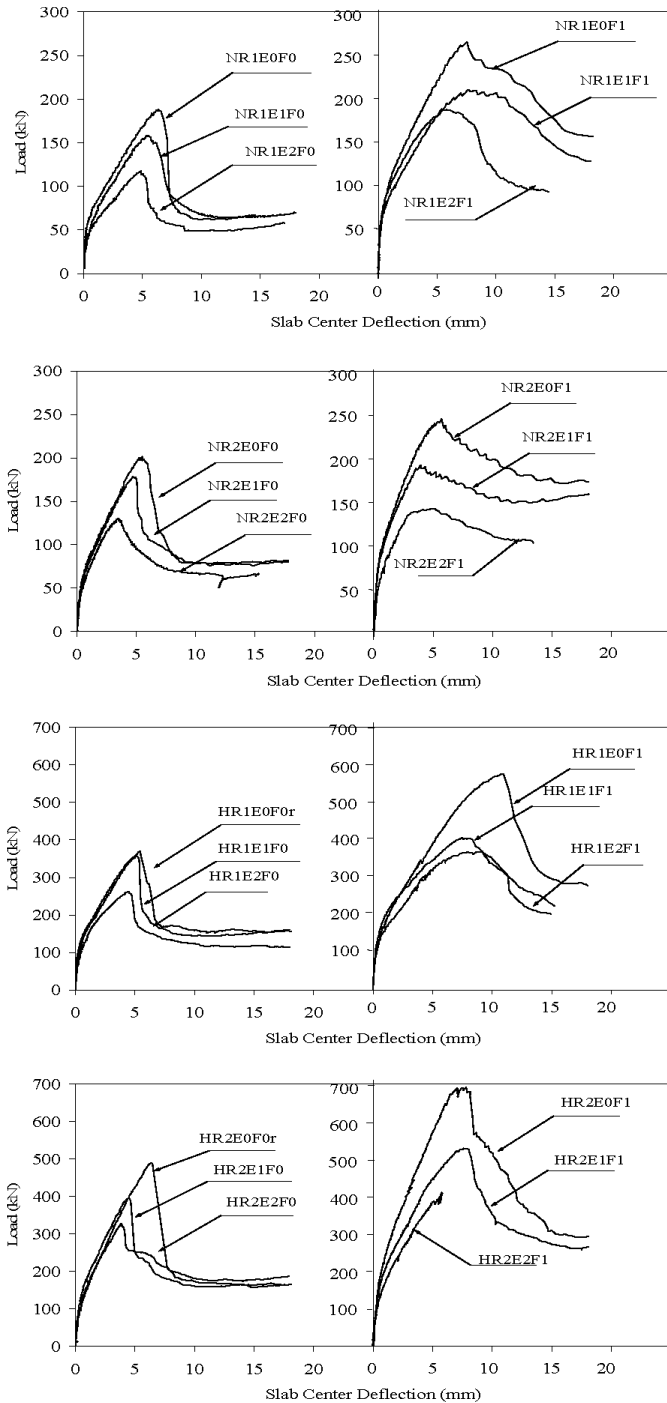


used (10 mm bars for NSC slabs and 14 mm bars for HSC slabs).

It was observed that the residual strength, P_{re} , decreased with an increase in eccentricity, and the addition of SFR to concrete resulted in a considerable increase in the residual load capacity.

Relatively stable residual load resistance promotes redistribution of stresses to adjacent slab–column connections, enabling reserve punching capacity. Further investigation of the importance of residual capacity is needed, however, since the P_{re}/P_p ratios were rather low for the slab specimens tested in the current study, as indicated in Table 2.

Fig. 7. Load – slab center deflection curves of specimens.



Effects of test parameters

Concrete strength

The concrete compressive strength had a significant effect on both the punching capacity and the load–deflection behavior of specimens. The initial and postcracking slopes of load–deflection curves (slab stiffness) are observed to be steeper in HSC specimens when compared with those of NSC slabs. Table 2 indicates that, beyond cracking, the ratio of tangent stiffnesses of companion HSC and NSC speci-

mens varies with the ratio of slab flexural capacity (m), where m is the flexural capacity of a unit width of slab with the effect of steel fiber included in the capacity calculations. The post-failure behavior of specimens was also influenced by the slab concrete strength. It was observed that the negative slope of the load–deflection curve beyond the failure point, P_p , became steeper as f'_c increased, resulting in more brittle failures in HSC specimens. The increase in punching capacity seemed to be proportional to the splitting cylinder tensile strength of concrete, f_{sp} . The splitting tensile strength values obtained from tests performed on 150 mm × 300 mm cylinders yield a good indication of the tensile and shear strengths of concrete. The f_{sp} values for NSC and HSC specimens without SFR may well be predicted by available equations. On the other hand, these equations underestimate the positive effect of SFR content. The following expression, derived from the experimental results of the current investigation, may be used to determine the splitting tensile strength of concrete with or without SFR:

$$[1] \quad f_{spc} = 0.51(f'_c)^{k_1} \quad \text{where } k_1 = 0.5 + V_{fF}f'_c/1000$$

where k_1 is a value representing the influence of the SFR ratio on concrete strength, on splitting. The calculated split tensile strength, f_{spc} , and the ratio of experimental to calculated values, f_{sp}/f_{spc} , for each specimen are given in Table 2.

Presence of SFR

The test results showed a favorable influence of SFR on both the behavior and punching strength of test specimens. Adding SFR to concrete not only increased the punching capacity, but also increased the deformability of slabs at and beyond the failure load, P_p . The slopes of descending branches of load–deflection curves were not as steep as those for specimens without SFR. This was true for both NSC and HSC specimens. The failure was less brittle and the crack spacing and crack widths were smaller. It can be concluded that the addition of SFR to slab concrete may be a practical and economical way of increasing punching capacity of slab–column connections, thereby improving the overall slab behavior. It is therefore recommended that further research be conducted to investigate the contributions of SFR, with additional tests with different SFR contents.

Flexural capacity of slab

The test results indicate that punching capacity, P_p , and residual strength, P_{re} , were influenced by flexural capacity, P_{flex} , calculated using the yield line theory. Test results in Table 1 reveal that the punching strength increased with an increase in flexural capacity, but the increase in P_p was not proportional to the increase in flexural strength. When the flexural capacity was increased by 50%, the punching capacity increased by approximately 10% and 20% in NSC and HSC specimens, respectively.

The flexural capacity of slabs also influenced stiffness within the postcracking range. The slopes of load–deflection curves in this range of deformations were steeper in specimens with higher flexural capacities, regardless of concrete strength and the eccentricity of load. The increase in flexural capacity also increased the residual strength, P_{re} .

Table 2. Comparison of calculated values for all specimens tested.

Specimen	m (kN·m/m)	k_{ct} (kN/mm)	k_{ct}/m	f_{spc} (MPa)	f_{sp}/f_{spc}	P_{re}/P_p	P_{rec} (kN)	P_{re}/P_{rec}	P_{CSA} (kN)	P_p/P_{CSA}
NR1E0F0	33.4	23.2	0.69	2.37	0.98	0.34	88.1	0.72	223	0.84
NR1E1F0	33.2	21.9	0.66	2.24	1.06	0.41	66.5	0.98	152	1.05
NR1E2F0	32.7	16.8	0.51	2.19	1.01	0.42	54.1	0.91	116	1.01
NR2E0F0	47.4	31.8	0.67	2.28	1.03	0.39	89.6	0.87	215	0.94
NR2E1F0	47.7	27.0	0.57	2.33	1.03	0.44	73.5	1.07	158	1.13
NR2E2F0	47.5	25.9	0.55	2.29	0.99	0.51	59.6	1.11	121	1.07
HR1E0F0	67.5	42.9	0.64	4.39	1.04	0.41	168.0	0.81	413	0.80
HR1E0F0r	67.6	53.0	0.78	4.42	1.12	0.43	169.0	0.94	416	0.89
HR1E1F0	67.6	54.4	0.80	4.42	1.12	0.41	139.0	1.05	299	1.19
HR1E2F0	67.6	37.7	0.56	4.42	1.12	0.45	117.0	1.01	234	1.12
HR2E0F0	96.0	79.8	0.83	4.07	1.01	0.43	165.0	1.06	383	1.06
HR2E0F0r	97.5	66.6	0.68	4.41	1.09	0.36	177.0	1.00	415	1.18
HR2E1F0	97.5	65.6	0.67	4.41	1.09	0.41	145.0	1.12	299	1.33
HR2E2F0	97.5	59.8	0.61	4.41	1.09	0.50	122.0	1.34	233	1.40
NR1E0F1	43.1	27.3	0.63	2.39	1.02	0.58	148.0	1.05	212	1.25
NR1E1F1	43.1	23.3	0.54	2.39	1.02	0.59	122.0	1.02	153	1.38
NR1E2F1	43.1	23.0	0.53	2.39	1.02	0.51	104.0	0.92	119	1.58
NR2E0F1	55.2	38.2	0.69	2.37	1.05	0.70	172.0	1.00	211	1.16
NR2E1F1	55.2	33.7	0.61	2.37	1.05	0.78	143.0	1.05	152	1.27
NR2E2F1	55.2	29.7	0.54	2.37	1.05	0.74	122.0	0.86	119	1.20
HR1E0F1	94.4	48.8	0.52	6.58	1.04	0.48	270.0	1.02	433	1.33
HR1E1F1	94.4	35.8	0.38	6.58	1.04	—	225.0	—	312	1.30
HR1E2F1	94.4	33.7	0.36	6.58	1.04	0.57	192.0	1.09	243	1.51
HR2E0F1	121.0	78.9	0.65	6.42	1.09	0.43	314.0	0.94	427	1.62
HR2E1F1	121.0	58.7	0.48	6.42	1.09	0.50	261.0	1.01	308	1.72
HR2E2F1	121.0	54.0	0.45	6.42	1.09	—	224.0	—	240	1.71

Note: Parameters as defined in the List of symbols.

Eccentricity of load

Specimens were tested under three different eccentricities of load, namely 0, 100, and 200 mm. The failure load, post-cracking stiffness, and residual load were observed to be influenced by the eccentricity of the applied load. With increasing eccentricity, a reduction in punching capacity was observed regardless of concrete strength, slab reinforcement ratio, and SFR content. In eccentrically loaded specimens, punching shear stresses increased due to the moment transfer. Therefore, the punching capacity decreased with an increase in eccentricity. The effect of the eccentricity of load on strength and deformability of slab specimens can be seen in Fig. 7. When SFR was not used, the reduction in punching capacity, P_p , with an increase in eccentricity was approximately the same for NSC and HSC specimens. At an eccentricity of 100 mm, NSC specimens failed at approximately 15% lower loads than those tested under concentric loading, because of moment transfers at plate-column connections. On the other hand, when the eccentricity was 200 mm, the strength decreased by about 35% as compared with slabs tested under concentric loading. The reduction in punching capacity with an increase in eccentricity was slightly less pronounced in HSC slabs. The addition of SFR resulted in higher reductions in punching capacity, P_p , with an increase in eccentricity. NSC specimens with SFR showed an average drop of about 22% in punching capacity when an eccentricity of 100 mm was employed.

The eccentricity of load also affected the crack pattern. In concentrically loaded specimens, the cracks occurred on all four sides of the column, whereas in eccentrically loaded

specimens the cracks concentrated near the column face in the direction of eccentricity. This is illustrated in Figs. 5 and 6. The residual strength, P_{re} , at which the post-failure load was stabilized was also influenced by eccentricity, in a similar manner.

Analytical investigation

Prediction of residual strength

Experimentally recorded test variables were used to derive empirical expressions to predict the residual load capacity, P_{re} , of slab specimens. Linear regression analysis was conducted using reinforcement yield strength (f_y), eccentricity of load (γ_r), concrete compressive strength (f'_c), total cross-sectional area of slab reinforcement crossing punching perimeter (A_s), and flexural capacity of a unit width of slab (m). Both slabs with and without SFR were considered, with appropriate concrete models used in the computation of the flexural capacity (m), incorporating the effects of SFR (Swamy and Al-Ta'an 1981). The resulting expressions for calculated residual strength (P_{rec}) are given as eqs. [2] and [3] for slabs without and with SFR, respectively. The factor accounting for the eccentricity of load (γ_r) is calculated in eq. [4], where J/b_1 is the section property of punching perimeter, as given in eq. [5]. All expressions are given for SI units.

$$[2] \quad P_{rec} = 1.15 \frac{A_s f_y \gamma_r \sqrt{f'_c}}{1000m} - 18 \quad (\text{without SFR})$$

$$[3] \quad P_{\text{rec}} = 2.30 \frac{A_s f_y \gamma_r \sqrt{f'_c}}{1000m} - 9 \quad (\text{with SFR})$$

$$[4] \quad \gamma_r = \frac{1}{1 + [u_p d(e/5)]/(J/b_1)}$$

$$[5] \quad J/b_1 = [b_1 d(b_1 + 3b_2) + d^3]/6$$

where J is the property of the punching perimeter analogues to the polar moment of inertia, b_1 is the dimension of the punch cone in the direction of eccentricity, b_2 is the dimension of the punch cone in the transverse direction to eccentricity, u_p is the perimeter length of the punch cone, and e is the eccentricity of the applied load. Calculated values of P_{rec} , based on eqs. [2] and [3], are listed in Table 2 for all specimens tested. The ratio of experimental to calculated values ($P_{\text{re}}/P_{\text{rec}}$) is also given in Table 2. In general, the ratios obtained are close to 1.00, indicating reasonably good predictions of experimental values with calculated ones, using eqs. [2]–[5]. It should be noted that the compression reinforcement was kept constant in the current study at 50% of tension reinforcement. Further testing with a wider range of variables is needed to verify the applicability of eqs. [2]–[5]. to slabs with parameters outside the range considered in the current experimental program.

Comparison of test results with Canadian Standards Association Standard CSA-A23.3-04

The punching shear clauses of Canadian Standards Association (CSA) Standard CSA-A23.3-04 (CSA 2004) are based on empirical expressions and incorporate only the effects of concrete strength, load eccentricity, location of the column, and punching cone aspect ratio. Of the test data used to verify the empirical equations in the CSA standard, only a small percentage was on high-strength concrete. Furthermore, the effect of SFR was not considered. Table 2 includes punching shear capacities computed on the basis of CSA-A23.3-04 clauses, P_{CSA} , with a material resistance factor taken as unity to obtain the nominal strength values. The ratios of experimental to calculated values (P_p/P_{CSA}) are also listed in Table 2. This ratio varies between 0.84 and 1.13 for NSC specimens and between 0.80 and 1.40 for HSC specimens, in the absence of SFR. They tend to become larger than unity for slabs with higher reinforcement ratios, indicating the positive influence of flexural slab reinforcement. The calculated concentric punching values are consistently higher than the experimental values for NSC and HSC slabs with low slab reinforcement ratios. It should be noted that the reinforcement index for these specimens is approximately $R_i = 0.85$, whereas it is about $R_i = 1.25$ for specimens with a high slab reinforcement ratio, regardless of concrete compressive strength. On the other hand, the experimental and CSA-A23.3-04 values are in good agreement with those for NSC and HSC specimens tested under eccentric loading, regardless of the reinforcement index, R_i . The experimental capacities of specimens with SFR are consistently higher than those computed based on CSA-A23.3-04, regardless of concrete strength and slab reinforcement ratio. The ratio of experimental values to CSA-A23.3-04 values varied between 1.16 and 1.58 for NSC specimens and between 1.30 and

1.72 for HSC specimens. These higher ratios are explained by the increase in tensile strength of concrete with the addition of SFR. The crack patterns shown in Figs. 5 and 6 also explain these high ratios. Furthermore, the confining effect of the undamaged portion of slabs is higher in specimens with SFR, where cracking is more restricted to a smaller region around column-to-plate connections.

Conclusions

The following conclusions are drawn from the experimental investigation presented in this paper, where all the slabs failed in punching shear:

- (1) The location of the critical perimeter for punching is not dependent on the parameters investigated in the experimental program, i.e., concrete strength, reinforcement ratio, presence of SFR, and eccentricity of loading. The critical failure crack was consistently located approximately 100 mm away from the column stub on the tension face, a distance equal to the effective slab depth.
- (2) Concrete strength has a direct influence on the punching behavior and punching capacity of concrete slabs. The initial and postcracking stiffnesses of HSC specimens tested were higher than those of NSC specimens.
- (3) Reinforced concrete slabs develop a relatively stable residual strength, P_{re} , after the initial punching failure. This was observed consistently in all concentric and eccentricity tested slabs. The expressions developed (eqs. [2] and [3]) provide good predictions of residual capacity of the tested specimens.
- (4) The addition of SFR to slab concrete significantly increases its punching capacity while reducing its brittleness. Slab specimens with NSC and HSC showed a more gradual failure when SFR is used. Moreover, the observed cracks were more closely spaced and concentrated near the column stub when SFR was used. The positive effect of SFR can be attributed to the increase in tensile strength of concrete and the increase in area of the undamaged portion of the plate resulting in a higher in-plane confining force on the plate-to-column connection.
- (5) The failure of HSC slabs is more brittle. The post-failure slopes of force–deformation relationships are steeper for the HSC specimens than for the NSC specimens.
- (6) Increasing the plate flexural reinforcement ratio results in an increase in the punching and residual strengths. The rate of increase in P_p is far lower than the increase in the slab flexural reinforcement ratio, however.
- (7) The CSA-A23.3-04 punching shear capacity predictions provide conservative estimates for concentrically loaded slabs and good predictions for eccentrically loaded slabs in the absence of SFR. When SFR is used, the CSA-A23.3-04 predictions are consistently conservative for all cases, as the approach does not include the effect of SFR in capacity calculations.

Acknowledgments

Funding provided by the Scientific and Technical Research Council of Turkey, TUBITAK (grant INTAG-509),

and the Bogazici University Research Fund (grant AFP-94A0420) are gratefully acknowledged.

References

- ACI Committee 318. 2002. Building code requirements for structural concrete (ACI 318-02). American Concrete Institute, Farmington Hills, Mich.
- Alexander, S.D.B., and Simmonds, S.H. 1992. Punching shear tests of concrete slab-column joints containing fiber reinforcement. *ACI Structural Journal*, **89**(4): 425–432.
- CED-fib Task Group. 2001. Punching of structural concrete slabs. Bulletin 12, Fédération Internationale du Béton (fib), Lausanne, Switzerland.
- CSA Committee A23.3. 2004. Design of concrete structures for buildings. Standard CSA-A23.3-04, Canadian Standards Association, Toronto, Ont.
- Gardner, N.J. 1990. Relationship of the punching shear capacity of reinforced concrete slabs with concrete strength. *ACI Structural Journal*, **87**(1): 66–71.
- Gardner, N.J., and Shao, X.-Y. 1996. Punching shear of continuous flat reinforced concrete slabs. *ACI Structural Journal*, **93**(2): 219–228.
- Ghalib, M.A. 1980. Moment capacity of steel fiber reinforced small concrete slabs. *ACI Journal*, **77**(4): 247–257.
- Gomes, R.B., and Andrade, M.A.S. 1996. The use of high performance concrete in punching failure of reinforced concrete flat slabs. *In Proceedings of the 4th International Symposium on the Utilization of High Strength/High Performance Concrete*, Paris, France, 29–31 May 1996. *Edited by* F. de Larrard and R. Lacroix. Laboratoire des Ponts et Chaussées, Paris. Vol. 3, pp. 1027–1035.
- Halgren, M., and Kinnunen, S. 1993. Punching shear tests on circular high strength concrete slabs. *In Utilization of High Strength Concrete, Proceedings of a Symposium*, Lillehammer, Norway, 20–23 June 1993. *Edited by* I. Holand and E. Sellevold. Norwegian Concrete Association, Oslo, Norway. pp. 192–199.
- Halgren, M., and Kinnunen, S. 1996. Increase of punching shear capacity by using high strength concrete. *In Proceedings of the 4th International Symposium on the Utilization of High Strength/High Performance Concrete*, Paris, France, 29–31 May 1996. *Edited by* F. de Larrard and R. Lacroix. Laboratoire des Ponts et Chaussées, Paris. Vol. 3, pp. 1037–1046.
- Hanson, N.W., and Hanson, J.M. 1968. Shear and moment transfer between concrete slabs and column. *Journal of the Portland Cement Association, Research and Development Laboratories*, **10**(1): 2–16.
- Hatcher, D.S., Sozen, M.A., and Siess, C.P. 1961. A study of tests on flat plate and a flat slab. Research Report, Civil Engineering Department, University of Illinois, Urbana, Ill.
- Hawkins, N.M., and Mitchell, D. 1979. Progressive collapse of flat plate structures. *ACI Journal, Proceedings*, **76**(7): 775–808.
- Lou, Y.H., and Durrani, A.J. 1995. Equivalent beam model for flat-slab buildings: Part I: interior connections. *ACI Structural Journal*, **92**(1): 115–124.
- Lovrovich, J.S., and McLean, D.I. 1990. Punching shear behavior of slabs with varying span-depth ratios. *ACI Structural Journal*, **87**(5): 507–512.
- Marzouk, H., and Hussein, A. 1991. Experimental investigation on the behavior of high-strength concrete slabs. *ACI Structural Journal*, **88**(6): 701–713.
- Mast, P.E. 1970. Stresses in flat plates near columns. *ACI Journal, Proceedings*, **67**(10): 761–768.
- Moe, J. 1961. Shearing strength of reinforced concrete slabs and footings under concentrated loads. Bulletin 47, Research and Development Laboratories, Portland Cement Association, Skokie, Ill.
- Moehle, J.P., Kreger, M.E., and Leon, R. 1988. Background to recommendations for design of reinforced concrete slab-column connections. *ACI Structural Journal*, **85**(6): 636–644.
- Neth, V.W., de Paiva, H.A.R., and Long, A.E. 1981. Behavior of models of a reinforced concrete flat plate edge-column connection. *ACI Journal, Proceedings*, **78**(4): 269–275.
- Ozden, S. 1998. Punching shear behavior of normal and high-strength concrete flat-plates. Ph.D. thesis, Department of Civil Engineering, Bogazici University, Istanbul, Turkey.
- Ozselcuk, A. 1980. Contribution of flexural steel to punching strength. M.S. thesis, Department of Civil Engineering, Middle East Technical University, Ankara, Turkey.
- Pan, A.D., and Moehle, J.P. 1992. Experimental study of slab-column connections. *ACI Structural Journal*, **89**(6): 626–638.
- Paramasivam, P., and Tan, K.H. 1993. Punching shear strength of ferrocement slabs. *ACI Structural Journal*, **90**(3): 294–301.
- Pecknold, D.A. 1975. Slab effective width for equivalent frame analysis. *ACI Journal, Proceedings*, **72**(4): 135–137.
- Ramdane, K.E. 1996. Punching shear of high performance slabs. *In Proceedings of the 4th International Symposium on the Utilization of High Strength/High Performance Concrete*, Paris, France, 29–31 May 1996. *Edited by* F. de Larrard and R. Lacroix. Laboratoire des Ponts et Chaussées, Paris. Vol. 3, pp. 1015–1026.
- Rao, G.R., and Goli, H.B. 1985. Yield line analysis of single panel flat slab. *International Journal of Structures*, **5**(1): 23–44.
- Shilling, R.C., and Vanderbilt, M.D. 1970. Behaviour of shear test structures. Structural Research Report 4, Civil Engineering Department, Colorado State University, Fort Collins, Colo.
- Swamy, R.N., and Ali, S.A.R. 1982. Punching shear behavior of reinforced slab-column connections made with steel fiber concrete. *ACI Journal, Proceedings*, **79**(5): 392–406.
- Swamy, R.N., and Al-Ta'an, S.A. 1981. Deformation and ultimate strength in flexure of reinforced concrete beams made with steel fiber concrete. *ACI Journal, Proceedings*, **78**(5): 395–405.
- Tankut, T., and Yu, C.W. 1969. An investigation into the behavior of flat plate structures. Research Report, Imperial College, London, UK.
- Theodorakopoulos, D.D., and Swamy, N. 1993. Contribution of steel fibers to the strength characteristics of lightweight concrete slab-column connections failing in punching shear. *ACI Structural Journal*, **90**(4): 342–355.
- Vanderbilt, M.D. 1972. Shear strength of continuous plates. *Journal of the Structural Division, ASCE*, **89**(5): 961–973.
- Zaghlool, E.R.F., and de Paiva, H.A.R. 1973. Test of flat plate corner column-slab connections. *Journal of the Structural Division, ASCE*, **99**(ST3): 551–572.

List of symbols

- A_s total area of slab reinforcement crossing the punching cone perimeter (mm^2)
- b_1 dimension of the punch cone in the direction of eccentricity (mm)
- b_2 dimension of the punch cone in the transverse direction to eccentricity
- d slab effective depth (mm)
- d' distance between compression bars and the extreme fiber in compression (mm)
- D_b diameter of slab flexural reinforcement (mm)
- e eccentricity of the applied load (mm)

f'_c	150 mm × 300 mm standard concrete cylinder compressive strength (MPa)	P_{flex}	slab flexural strength obtained from the yield line analysis (kN)
f_{sp}	split cylinder strength (on 150 mm × 300 mm concrete cylinders) (MPa)	P_p	punching shear capacity of slab (kN) (experimental)
f_{spc}	calculated split cylinder strength (MPa)	P_{re}	experimental slab post-failure residual load capacity (kN)
f_y	yield strength of slab reinforcement (MPa)	P_{rec}	calculated slab post-failure residual load capacity (kN)
J	property of the punching perimeter analogous to the polar moment of inertia (mm ⁴)	R_i	reinforcement index ($R_i = \rho f_y / (f'_c)^{1/2}$)
k_{ct}	tangent stiffness after cracking (kN/mm)	s	spacing of slab tension reinforcement (mm)
k_1	value representing the influence of the SFR ratio on concrete strength, on splitting	s'	spacing of slab compression reinforcement (mm)
m	flexural capacity of a unit width of slab (kN·m/m)	t	thickness of the slab (mm)
P_{ACI}	calculated punching capacity of slab according to ACI 318-02 ($(f'_c)^{1/2} < 8.3$ MPa)	u_p	perimeter length of the punch cone (mm)
P_{cr}	flexural cracking load (kN)	V_{FF}	volume fraction of SFR in concrete mix (%)
P_{CSA}	calculated punching shear capacity on the basis of CSA-A23.3-04 clauses	γ_r	factor accounting for load eccentricity
		δ_{cr}	net vertical slab center deflection at cracking load, P_{cr} (mm)
		δ_p	net vertical slab center deflection at failure load, P_p (mm)
		ρ	ratio of slab tension reinforcement (%)

Copyright of Canadian Journal of Civil Engineering is the property of NRC Research Press and its content may not be copied or emailed to multiple sites or posted to a listserv without the copyright holder's express written permission. However, users may print, download, or email articles for individual use.

Canadian Journal of Civil Engineering

Volume 33, Number 11, November 2006
ISSN 1208-6029

Evaluation of sediment control pond performance at construction sites in the Greater Toronto Area

B.Gharabaghi, A.Fata, T.Van Seters, R.P. Rudra, G.MacMillan, D.Smith, J.Y. Li, A.Bradford, and G.Tesa

Pages 1335-1344

[Abstract](#) | [Full text \(PDF 1240 kb\)](#) | [Orders and Permissions](#)

Integration of field and laboratory testing to determine the causes of a premature pavement failure

Dar Hao Chen, Tung-Tsan Chen, Tom Scullion, and John Bilyeu

Pages 1345-1358

[Abstract](#) | [Full text \(PDF 1747 kb\)](#) | [Orders and Permissions](#)

Assessment of precast stringer highway bridges using mean load method

Daman K. Panesar and F.Michael Bartlett

Pages 1359-1367

[Abstract](#) | [Full text \(PDF 684 kb\)](#) | [Orders and Permissions](#)

Load and resistance data for precast stringer highway bridges

Daman K. Panesar and F.Michael Bartlett

Pages 1368-1378

[Abstract](#) | [Full text \(PDF 102 kb\)](#) | [Orders and Permissions](#)

Prediction of pressure fluctuations on sloping stilling basins

A.Güven, M.Günel, and A.Çevik

Pages 1379-1388

[Abstract](#) | [Full text \(PDF 490 kb\)](#) | [Orders and Permissions](#)

Punching shear tests of normal- and high-strength concrete flat plates

Sevket Ozden, Ugur Ersoy, and Turan Ozturan

Pages 1389-1400

[Abstract](#) | [Full text \(PDF 1095 kb\)](#) | [Orders and Permissions](#)

A comparison of two regional seismic damage estimation methodologies

Tuna Onur, Carlos E. Ventura, and W.D. Liam Finn

Pages 1401-1409

[Abstract](#) | [Full text \(PDF 303 kb\)](#) | [Orders and Permissions](#)

Effect of aggregate type, gradation, and compaction level on thermal properties of hot-mix asphalts

Donath M. Mrawira and Joseph Luca

Pages 1410-1417

[Abstract](#) | [Full text \(PDF 401 kb\)](#) | [Orders and Permissions](#)

Digital image correlation analysis of crack behavior in a reinforced concrete beam during a load test

Michel Küntz, Marc Jolin, Josée Bastien, Fabien Perez, and François Hild

Pages 1418-1425

[Abstract](#) | [Full text \(PDF 587 kb\)](#) | [Orders and Permissions](#)

Investigation of bond between fibre-reinforced polymer bars and concrete under sustained loads

F.Shahidi, L.D. Wegner, and B.F. Sparling

Pages 1426-1437

[Abstract](#) | [Full text \(PDF 1284 kb\)](#) | [Orders and Permissions](#)

Experimental study on the behavior of carbon fiber reinforced polymer sheets bonded to concrete

Ayman S. Kamel, Alaa E. Elwi, and Roger J.J Cheng

Pages 1438-1449

[Abstract](#) | [Full text \(PDF 1116 kb\)](#) | [Orders and Permissions](#)

Nonlinear cash flow optimization model

Jaeho Son, Martin Mack, and Kris G. Mattila

Pages 1450-1454

[Abstract](#) | [Full text \(PDF 142 kb\)](#) | [Orders and Permissions](#)

Characteristics of volcanic ash and natural lime based stabilized clayey soils

K.M.A Hossain, M.Lachemi, and S.Easa

Pages 1455-1458

[Abstract](#) | [Full text \(PDF 51 kb\)](#) | [Orders and Permissions](#)

[How to View a PDF](#)

Date Modified: 2007-05-22

Canadian Journal of Civil Engineering



Contents

[Current issue \(vol. 35, issue 1\)](#)

[Advance online issue\(s\)](#) **RSS**

[Previous issues](#)

[Sample issue](#)

Published since 1974, this monthly publication is the official journal of the Canadian Society for Civil Engineering. It contains articles on environmental engineering, hydrotechnical engineering, structure engineering, construction engineering, engineering

mechanics, and engineering materials, and a history of civil engineering. Contributors include recognized researchers and practitioners in industry, government, and academe. New developments in engineering design and construction are also featured.

Information & Services

ISSN: 1208-6029

[Information for authors](#)

[Submit an article](#)

Subscribe to a journal ([2007](#), [2008](#))

[Sign up for RSS feeds](#)

[Sign up for publication alerts](#)

Affiliations

[The Canadian Society for Civil Engineering](#) has chosen the *Canadian Journal of Civil Engineering* as its principal medium of publication of engineering papers.

Editor



Dr. Don Mavinic — The University of British Columbia, Vancouver, British Columbia, Canada

Dr. Mavinic is full professor of Civil and Environmental Engineering at the University of British Columbia and Head of the university's Environmental Engineering group. He is a Professional Engineer in British Columbia, as well as a Fellow of the Canadian Society for Civil Engineering, the Engineering Institute of Canada, and the Canadian Academy of Engineering. He has published more than 200 papers and technical reports — more than half of them in peer-reviewed journals.

Associate Editors

F.M. Bartlett (London), N. Biswas (Windsor), A.M. da Silva (Kingston), S. Foo (Gatineau), P. Gauvreau (Toronto), F. Hicks (Edmonton), K. Khayat (Sherbrooke), M. Lachemi (Toronto), R. Loov (Calgary), D.B. MacFarlane (Fredericton), C. Marche (Montréal), B. McCabe (Toronto), S. Mindess (Vancouver), B. Morse (Sainte-Foy, QC), J. Proulx (Sherbrooke), J. Rankin (Fredericton), C.A. Rogers (Montréal), A.D. Russell (Vancouver), F. Saccomanno (Waterloo), T. Sayed (Vancouver), N. Shrive (Calgary), D.F.E. Stolle (Hamilton), S.I. Tighe (Waterloo), L.M. Waugh (Fredericton), R.G. Zytner (Guelph)

Assistant to the Editor

Kelly Lamb — The University of British Columbia

Editorial office

Canadian Journal of Civil Engineering, Department of Civil Engineering, The University of British Columbia, Vancouver, BC V6T 1Z4 Canada

Tel.: 604-822-2523

Fax: 604-822-0568

Email: cjce@civil.ubc.ca

Indexed in

Abstract Journal in Earthquake Engineering; Applied Science and Technology Abstracts; Applied Science and Technology Index; Current Contents; Engineering Index; ETDE Energy Database; Fluidex; GEOBASE; GeoRef; Hydrofind; International Civil Engineering Abstracts; Science Citation Index

Publisher

Managing Editor	Bushra Waheed 613-993-0369
Publication Officers	Lesia Beznaczuk, Jenny Ryan
Editorial Publication Assistants	Olivier Nguyen-Huu
Desktop Publishing Technician	Stephen Brossoit
Graphics Technician	Dario Ferrara
Web Technician	Angela Lamarche

Date Modified: 2008-01-17